ISSN 0030-400X, Optics and Spectroscopy, 2016, Vol. 120, No. 1, pp. 28–37. © Pleiades Publishing, Ltd., 2016.
Original Russian Text © D.K. Tuchina, V.D. Genin, A.N. Bashkatov, E.A. Genina, V.V. Tuchin, 2016, published in Optika i Spektroskopiya, 2016, Vol. 120, No. 1, pp. 36–45.

OPTICS AND SPECTROSCOPY IN BIOPHYSICS AND MEDICINE

Optical Clearing of Skin Tissue ex vivo with Polyethylene Glycol

D. K. Tuchina[a], V. D. Genin[a], A. N. Bashkatov[a, b], E. A. Genina[a, b], and V. V. Tuchin[a, b, c]

[a] *Chernyshevskii Saratov State University, Saratov, 410012 Russia*

[b] *Tomsk State University, Tomsk, 634050 Russia*

[c] *Institute of Precision Mechanics and Control, Russian Academy of Sciences, Saratov, 410028 Russia*

e-mail: tuchinadk@mail.ru

Received August 16, 2015

Abstract—Alterations of the optical and structural (weight, thickness, and square) parameters of skin caused by polyethylene glycol (PEG) with molecular weights of 300 and 400 Da were studied experimentally. The objects of the study were ex vivo skin samples of albino laboratory rats. Collimated transmittance of the skin was measured in the wavelength range 500–900 nm. As a result of exposure to the agents, an increase in the collimated transmittance and a decrease in weight, thickness, and square of skin samples were observed. Analysis of the kinetics of parameters alterations allowed us to measure the diffusion coefficient of the agents in the skin as $(1.83 \pm 2.22) \times 10^{-6}$ and $(1.70 \pm 1.47) \times 10^{-6}$ cm^2/s for PEG-300 and PEG-400, respectively, and the rate of alterations of the structural parameters. The results obtained in this study can be used for the improvement of existing and development of new methods of noninvasive diagnostics and therapy of subcutaneous diseases.

DOI: 10.1134/S0030400X16010215

INTRODUCTION

Since the optical methods of diagnostics and treatment of various diseases are relatively inexpensive and safe for the health of patients, they are currently actively used in medicine [1–3]. However, the delivery of sensing radiation through the surface of biological tissues to the required depth is one of the main problems in modern laser medicine. The difficulty of solving this problem is determined by the fact that the spatial resolution and depth of sensing with radiation in the visible and near-infrared spectral regions are strongly limited by the scattering ability of biological tissues [3]. Since the main cause of optical radiation scattering in tissues is the difference between the refractive indices of the structural components of biological tissues and the interstitial fluid or intracellular organelles and cytoplasm [3], a possible solution to this problem may be to reduce light scattering by replacing the interstitial fluid with a biocompatible immersion agent (i.e., the use of the so-called "optical clearing of biological tissues" procedure [3–7]).

Currently, the decrease in the light scattering of biological tissues under exposure to optical clearing agents (OCAs) is believed to be due to three main processes: osmotic dehydration of biological tissue, partial replacing the interstitial fluid with the immersion agent, and structural modification or dissociation of collagen fibers of biological tissue [5–11]. The first two processes usually occur simultaneously. The contribution of each of them to the clearing effect is determined by the type of OCA and the properties of biological tissue. The effect of the third process becomes noticeable only after long-term exposure of biological tissue to OCA.

Due to its effectiveness, availability, and biocompatibility, polyethylene glycol can be successfully used as a OCA [12–17]. Polyethylene glycol (abbreviated PEG chemical formula $C_{2n}H_{4n+2}O_{n+1}$) is a polymer of ethylene glycol ($C_2H_6O_2$) belonging to the class of diols. Depending on the molecular weight, polyethylene can be a viscous liquid, gel, or solid. PEG-300 and PEG-400 are transparent, viscous, colorless liquids with a molecular weight of 300 and 400 Da and exhibit strong hygroscopic properties decreasing with increasing molecular weight [18, 19]. Polyethylene glycol is actively used in medicine and cosmetology as a basis for ointments and was registered as a food additive E1521. It is also used as a solvent, extractant, preservative, and strong osmotic agent [18].

Information about the diffusion coefficients of a OCA in biological tissues and the processes taking place during the interaction of a OCA with a biological tissue can be used to develop new and optimize existing methods of optical clearing of tissues. Previously, the diffusion coefficients of PEG-300 and PEG-400 were measured in the stratum corneum of the skin [20], in the cornea and conjunctiva of the eye, and in agarose gel simulating an epithelial membrane. However, despite the fairly wide use of PEG booth in cosmetology and as a clearing agent, the analysis of the

Table 1. Refractive indices of PEG-300 and PEG-400 measured at different wavelengths

λ, nm	450	480	486	546	589	644	656	680	930	1100	1300	1550
PEG-300	1.4709	1.4685	1.4682	1.4650	1.4631	1.4610	1.4604	1.4596	1.4559	1.4544	1.4501	1.4460
PEG-400	1.4733	1.4708	1.4706	1.4670	1.4649	1.4633	1.4627	1.4620	1.4581	1.4567	1.4526	1.4483

Table 2. Interpolation coefficients of the spectral dependence of the refractive index of PEG-300 and PEG-400

	a_0	a_1	a_2	a_3	a_4	a_5	a_6	a_7
PEG-300	0.23858	0.02777	-2.28051×10^{-3}	-6.28375×10^{-4}	4.23549×10^{-3}	−88.63291	-5.08374×10^{4}	−0.02324
PEG-400	0.23821	0.02743	-2.6284×10^{-3}	-6.05667×10^{-4}	4.28405×10^{-3}	−68.04619	-3.85264×10^{4}	−0.02098

available literature showed that diffusion of PEG-300 and PEG-400 in skin tissues has been studied insufficiently [14, 20–23].

The aim of this study was to investigate the time dependence of alterations of the optical, weight, and geometrical parameters of the skin ex vivo under exposure to PEGs and to measure the diffusion coefficients of PEG-300 and PEG-400 in skin tissues.

MATERIALS AND METHODS

Study Objects and Optical Clearing Agents

The study was performed ex vivo on 80 skin samples of albino laboratory rats (ten samples to study the kinetics of alteration of each parameter: collimated transmittance, weight, thickness, and square for each test agent). Before the experiments, hair from the skin was removed using Veet depilatory cream (Reckitt Benckiser, France). Pieces approximately 10 × 15 mm were excised from the skin samples with surgical scissors. The subcutaneous fat layer preventing the penetration of hydrophilic substances into the derma was removed.

Polyethylene glycol-300 (PEG-300, molecular weight 300 Da, Sigma-Aldrich, Germany) and polyethylene glycol-400 (PEG-400, molecular weight 400 Da, Sigma-Aldrich, Belgium) were used as OCAs. PEG-300 had a density of 1.125 g/mL and a viscosity of approximately 95 g/(m s) [24], while PEG-400 had a density of 1.126 g/mL and a viscosity of approximately 120 g/(m s) [25]. The osmotic pressure of the solutions was calculated using the equation [26]

$$P = \alpha C + \beta C^2,$$

where R is the osmotic pressure (MPa) and C is the molar concentration (mol/L). For PEG-300: $\alpha = 1.7$, $\beta = 3.3$; for PEG-400: $\alpha = 1.6$, $\beta = 5.0$ [26]. Given that $C_{\text{PEG-300}} = 3.750$ mol/L and $C_{\text{PEG-400}} = 2.815$ mol/L, the osmotic pressure of PEG-300 and PEG-400 is 52.8 and 44.1 MPa, respectively.

The dependence of the diffusion coefficient of PEG in water (in cm^2/s) on the molecular weight M_w at low concentrations is described, according to [27], by the expression $D_0(M_w) = 7\times10^{-9} M_w^{-0.46}$. This implies that D_0 for PEG-300 is 5.08×10^{-6} cm^2/s and D_0 for PEG-400 is 4.45×10^{-6} cm^2/s.

The refractive indices of OCAs were measured with an Abbe DR-M2/1550 multiwavelength refractometer (ATAGO, Japan) at 12 wavelengths in the range from 450 to 1550 nm and then interpolated. The results of measurements are summarized in Table 1. The interpolation was performed using the expression [28]

$$\frac{n^2-1}{n^2+1}\frac{1}{\rho^*} = a_0 + a_1\rho^* + a_2T^* + a_3\lambda^{*2}T^* + \frac{a_4}{\lambda^{*2}} + \frac{a_5}{\lambda^{*2}-\lambda_{\text{UV}}^{*2}} + \frac{a_6}{\lambda^{*2}-\lambda_{\text{IR}}^{*2}} + a_7\rho^{*2},$$

where n is the refractive index of PEG, $\rho^* = \rho/\rho_0$ is the relative density of the clearing agent, $\rho_0 = 1$ g/mL, $\lambda^* = \lambda/\lambda_0$ is the relative wavelength, $\lambda_0 = 589$ nm, $\lambda_{\text{UV}} = 229.202$ nm, $\lambda_{\text{IR}} = 5432.937$ nm, λ is the wavelength (nm), $T^* = T/T_0$ is the relative temperature of the clearing agent, and $T_0 = 273.15$ K. Table 2 summarized the interpolation coefficients for the clearing agents.

Measurements of Weight and Geometrical Parameters of Skin

The thickness of the samples was measured with a micrometer with an accuracy of ±10 μm. Each sample was placed between two slides, and the thickness was measured at five points; the results were averaged.

Weight was measured with electronic scales (Scientech, SA210, United States) with an accuracy of ±1 mg.

To calculate the square of a sample, it was placed on a test object with a scale bar and photographed with a digital camera. The coefficient of transition from the linear dimensions in pixels to the linear dimensions in millimeters was calculated using the scale bar, and the size of the entire image was determined. Then, the blue component (Fig. 1b) was isolated from the full-color image (Fig. 1a) as the most contrast one, which

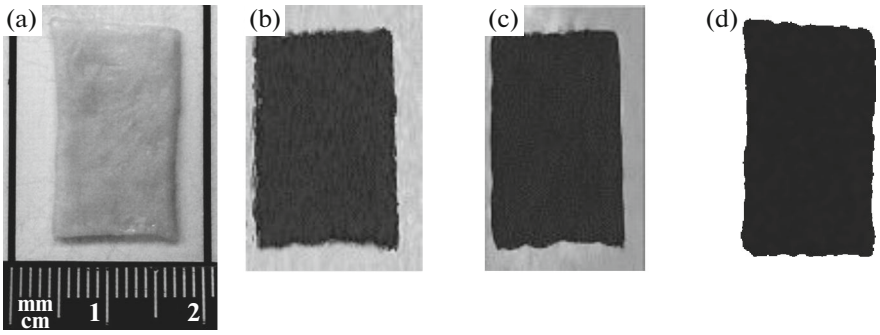

Fig. 1. (a) The image of a biological tissue sample on a test object, (b) the blue component of the skin sample image, (c) the image after the processing with the median filter, and (d) the result of digital image processing.

was processed with a median filter to remove the noise and glare (Fig. 1c). Since the brightness of pixels of the background (in the analysis of the blue components of the image) was higher than the brightness of pixels of the skin sample, all pixels with a certain threshold brightness (in our case, in the range of 190–200 units) was assigned a value of 255 (Fig. 1d). The number of pixels occupied by the sample (with values different from 255) was counted and converted into square millimeters using equation

$$S = \frac{F(H_s)}{cols(H_S)rows(H_S)} \frac{rows(H)z^2}{cols(H)},$$

where F is the number of pixels occupied by the sample, $cols$ is the number of columns, $rows$ is the number of rows, H_S is the image of the sample on a white background, H is the original image, and z is the width of the image.

To measure the kinetics of alteration of the thickness, square, and weight, all skin samples were placed in a Petri dish filled with a OCA. Each parameter was measured first before placing the samples in the OCA and then every 5–10 min after placing them in the OCA for 1.5–2 h of immersing.

Measurement of the Kinetics of Collimated Transmission of Skin Samples

The collimated transmittance spectra of the skin samples were recorded with a USB4000-Vis-NIR spectrometer (Ocean Optics, United States). The skin sample was mounted on a plate (38 × 17 mm) with an aperture (8 × 8 mm) and placed in a 5-mL glass cuvette filled with OCA. The cuvette was placed between two 400-μm optical fibers P400-1-UV-VIS (Ocean Optics, United States). To ensure the collimation of the beam, 74-ACR collimators were fixed at the ends of fibers using the standard connectors SMA-905 (Ocean Optics, United States). An HL-2000 halogen lamp (Ocean Optics, United States) was used as a radiation source. The experimental device is shown in Fig. 2.

The kinetics of alteration of collimated transmittance was recorded by sequentially recording the collimated transmittance spectra in the range of 500–900 nm every 5–10 min for 1.5–2 h. All measurements were performed at room temperature (~20°C).

Estimation of Diffusion Coefficients of OCA in Skin

It is well known that the diffusion of a hyperosmotic agent whose refractive index is greater than that of the interstitial fluid into a biological tissue and the efflux of water from the biological tissue leads to the concordance of refractive indices of scatterers and interstitial fluid, denser packing of components of the biological tissue, and, therefore, a reduction in the scattering coefficient [4–7, 29].

The method of estimation of diffusion coefficients of immersion liquids in biological tissue is based on the analysis of the kinetics of alteration of the collimated transmittance of biological tissue samples placed in a OCA, which changes as a result of the osmotic effect of the OCA and its diffusion into the

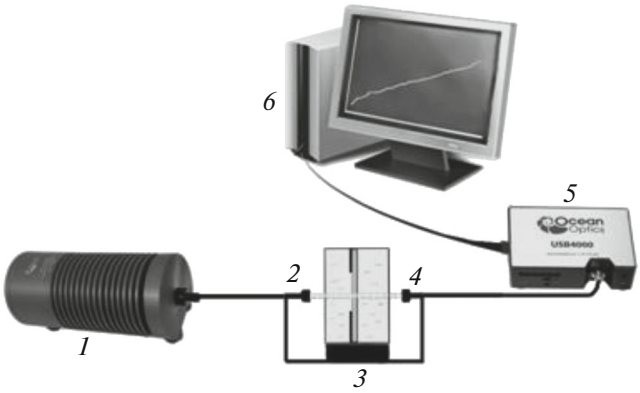

Fig. 2. Experimental device for the measurement of the collimated transmittance of skin samples. Designations: (*1*) HL-2000 halogen lamp, (*2, 4*) optical fibers with collimators, (*3*) cuvette with the sample, (*5*) USB4000-Vis-NIR spectrometer, and (*6*) personal computer.

biological tissue [29, 30]. The diffusion coefficient in this case is the mean flow rate of the exchange flux of the OCA into biological tissue and the efflux of water from the biological tissue.

The transport of immersion liquids in fibrous tissues can be described under a free-diffusion model. Geometrically, a biological tissue sample can be represented as a plane-parallel plate of finite thickness l (cm) consisting of scattering dielectric cylinders (collagen and elastin fibers). A one-dimensional diffusion equation can be written as [29, 30]

$$\frac{\partial C(x,t)}{\partial t} = D\frac{\partial^2 C(x,t)}{\partial x^2}, \tag{1}$$

where $C(x, t)$ is the OCA concentration in the skin (g/mL), D is the diffusion coefficient (cm^2/s), t is the diffusion time (s), and x is the spatial coordinate in the skin sample thickness (cm).

Since the OCA volume (~5000 mm^3) in the cuvette is much greater than the skin sample volume (~100–150 mm^3), it can be assumed that the penetration of PEG into the skin sample does not change the OCA concentration in the cuvette. The OCA penetrates into the skin primarily from the derma, which can be explained by the protective properties of the epidermis, preventing the penetration of OCA molecules into the skin. For one-directional diffusion, the boundary conditions are as follows:

$$C(0,t) = C_0 \quad \text{and} \quad \frac{\partial C(l,t)}{\partial x} = 0, \tag{2}$$

where C_0 is the concentration of PEG in the cuvette (g/mL). The second boundary condition reflects the fact that the diffusion of immersion liquid into the sample skin occurs from only one side of the sample (i.e., from the derma).

The initial conditions reflect the absence of OCA at all internal points of the biological tissue sample before placing the latter in the solution:

$$C(x,0) = 0. \tag{3}$$

The solution of Eq. (1) with allowance for the boundary (2) and entry (3) conditions takes the form

$$C(x,t) = C_0\left(1 - \sum_{i=0}^{\infty}\frac{4}{\pi(2i+1)}\sin\left(\frac{(2i+1)\pi x}{2l}\right) \times \exp\left(-\frac{(2i+1)^2 D\pi^2 t}{4l^2}\right)\right).$$

The mean concentration of OCA in the skin sample $C(t)$ at each time point is determined by the expression

$$C(t) = C_0\left(1 - \frac{8}{\pi^2}\sum_{i=0}^{\infty}\frac{1}{(2i+1)^2} \times \exp\left(-(2i+1)^2 t\frac{\pi^2}{4}D\Big/l^2\right)\right). \tag{4}$$

In a first approximation, Eq. (4) can be written as

$$C(t) \approx C_0(1 - \exp(-t / \tau_D)), \tag{5}$$

where

$$\tau_D = \frac{4l^2}{\pi^2 D}. \tag{6}$$

τ_D is the characteristic diffusion time.

The penetration of the immersion liquid into the skin is accompanied by a gradual increase in the refractive index $n_I(t)$ of the interstitial fluid. The time dependence of the refractive index of the interstitial fluid can be estimated on the basis of the Gladstone and Dale law [31], which, in the case of two-component solutions, takes the form

$$n_I(\lambda,t) = n_{I0}(\lambda)(1 - C(t)) + n_{PEG}(\lambda)C(t), \tag{7}$$

where λ is the wavelength (nm) and $n_{I0}(\lambda)$ is the refractive index of the interstitial fluid of the skin at the initial time, which depends on the wavelength [32]:

$$n_{I0}(\lambda) = 1.351 + \frac{2134.2}{\lambda^2} + \frac{5.79\times10^8}{\lambda^4} - \frac{8.15\times10^{13}}{\lambda^6}, \tag{8}$$

$n_{PEG}(\lambda)$ is the spectral dependence of the refractive index of PEG.

Since the thickness of the derma is dominant with respect to the thickness of other layers of the skin, the optical characteristics of the skin are determined primarily by the optical characteristics of the derma. The spectral dependence of the refractive index of collagen fibers has the form [33]

$$n_s(\lambda) = 1.439 + \frac{15880.4}{\lambda^2} - \frac{1.48\times10^9}{\lambda^4} + \frac{4.39\times10^{13}}{\lambda^6}. \tag{9}$$

The alteration of the scattering coefficient of the skin were quantified using the following equation [29, 30, 34]:

$$\mu_S(\lambda,t) = \frac{\varphi_S(t)}{\pi a^2}\sigma_S(\lambda,t)\frac{(1-\varphi_S(t))^3}{1+\varphi_S(t)}, \tag{10}$$

where $\varphi_S(t)$ is the volume fraction of scatterers dependent on time, a is the radius of scatterers, and $\sigma_S(\lambda,t)$ is the scattering cross section dependent on time [35]:

$$\sigma_S(\lambda,t) = \frac{\pi^2 a x^3(\lambda,t)}{8}(m^2(\lambda,t)-1)^2 \times\left(1+\frac{2}{(m^2(\lambda,t)+1)^2}\right), \quad (11)$$

where $m(\lambda,t) = n_S(\lambda)/n_1(\lambda,t)$ is the relative refractive index of scattering particles, which is determined using Eqs. (7) and (9), and $x(\lambda, t) = 2\pi a n_1(\lambda,t)/\lambda$ is the relative size of scatterers.

The value of the volume fraction of scatterers φ_{S0} at the initial time point was derived from the initial weight and volume of the samples using the relation

$$\begin{cases} W_s + W_{ICF} = W_0 \\ V_s + V_{ICF} = V_0 \end{cases} = \begin{cases} V_s\rho_s + V_{ICF}\rho_{ICF} = W_0, \\ V_s + V_{ICF} = V_0, \end{cases} \quad (12)$$

where W_s is the weight of scatterers of the skin; W_{ICF} is the weight of the interstitial fluid of the skin; V_s is the volume occupied by the scatterers of the skin; W_{ICF} is the volume occupied by the interstitial fluid of the skin; W_0 and V_0 are the weight and volume, respectively, of the sample measured at $t = 0$; $\rho_s = 1.41$ g/mL [36, 37]; and $\rho_{ICF} \approx 1$ g/mL is the density of the scatterers and the interstitial fluid of the skin. It follows from Eq. (12) that $V_s = V_0 - \dfrac{V_0\rho_s - W_0}{\rho_s - \rho_{ICF}}$ and $\varphi_{S0} = V_s/V_0$. The measured φ_{S0} values ranged from 0.2 to 0.25.

The alterations of the thickness $l(t)$ and square $S(t)$ of skin samples were used to account for the alteration of the volume fraction of diffusers during the clearing process $\varphi_S(t)$: $\varphi_S(t) = \varphi_{S0}V_0/V(t)$, where $V_0 = S_0 l_0$ and $V(t) = S(t)l(t)$.

The effective sizes of the skin scatterers were estimated on the basis of the collimated transmittance $T(t = 0)$ measured at the initial time. Since

$$\mu_{S0} = -\frac{\ln(T(t=0))}{l_0} - \mu_{a0}, \quad (13)$$

where μ_{a0} is the absorption coefficient of native skin [38], μ_{S0} is the scattering coefficient at the initial time, and l_0 is the initial thickness of the sample, the mean diameter of collagen fibers was found from the initial value of the scattering coefficient using Eqs. (10) and (11). The mean diameter $2a$ for different samples was 80–150 nm, which agrees well with the values of the diameter of the collagen fibers of human skin (40–150 nm) determined by electron microscopy [39]. When performing the calculations, we assumed that diameter of scatterers of the skin does not change under the action of PEG during the measurements.

To analyze the kinetics of alterations of the weight $W(t)$, thickness $l(t)$, square $S(t)$, and volume $V(t)$ of skin samples, the following equation was used:

$$\frac{A(t)}{A(t=0)} = B\exp(-t/\tau) + B_0, \quad (14)$$

where $A(t = 0)$ is the thickness, square, or weight of the sample measured at the initial time (volume was determined as the product of the square by the thickness) τ is the characteristic time of dehydration, B is the coefficient characterizing the degree of dehydration, and B_0 characterizes the residual value of the weight, square, volume, or thickness of the sample after dehydration.

The alteration of the absorption coefficient $\mu_a(t)$ was taken into account using the equation

$$\mu_a(t) = \varphi_S(t)\sigma_{a0}/\pi a^2, \quad (15)$$

where σ_{a0} is the absorption cross section, which is determined from the values μ_{a0} and φ_{S0}.

The time dependence of the coefficient of collimated transmittance of the skin sample placed in OCA has the form

$$T_c(t) = \exp[-(\mu_a(t) + \mu_S(t))l(t)]. \quad (16)$$

Equations (1)–(16) form the direct problem, i.e., determine the dependence of the coefficient of collimated transmittance on the concentration of the OCA solution in the skin sample. The inverse problem is to reconstitute the diffusion coefficient value by the time dependence of collimated transmittance. The solution of this problem requires minimizing the target functional:

$$f(D) = \sum_{i=1}^{N_t}(T_c(D,t_i) - T_c^*(t_i))^2,$$

where N_t is the total number of experimental points obtained during the recording of the time dependence of collimated transmittance at a fixed wavelength, $T_c(D,t)$ is the transmittance value calculated using Eq. (16) at time t for a given value D, and $T_c^*(t)$ is the experimentally measured transmittance at time t. Minimization was performed using the simplex method described in detail in [40].

It should be noted that, in Eq. (16), absorption and scattering coefficients are taken as spatially homogeneous for each time point. This assumption is true, because the attenuation coefficient in the course of measurements is automatically averaged along the collimated beam of light crossing the sample. Thus, the measured kinetics describes the behavior of a spatially averaged attenuation coefficient with the predominance of the scattering coefficient ($\mu_a \ll \mu_s$) in it.

RESULTS AND DISCUSSION

Figure 3 shows the kinetics of alterations of the weight, thickness, square, and volume of skin samples placed in PEG-300 and PEG-400. The experimental data were normalized to the values measured at the initial time point, averaged over all samples, and then approximated by Eq. (14). It can be seen from Figs. 3a–3d that, in both cases, all measured parameters are reduced: after 120 min of dehydration in the presence of PEG-300 and PEG-400, the weight of all samples decreased by approximately 32 and 37%, respectively; the thickness, by 30 and 38%; the square, by 24 and 30%; and the volume, by 47 and 56%.

The results of the analysis of the kinetics of dehydration using Eq. (14) are shown in Table 3. As can be seen from Fig. 3 and Table 3, despite the fact that PEG-330 and PEG-400 are similar, their effects on the degree of dehydration of the skin are different. For the total measurement time (approximately 2 h), PEG-400 caused greater dehydration of the skin, whereas PEG-300 was more effective during the first 30 min of exposure (cf. Figs. 3a, 3c, 3d), which was associated with its lower viscosity and greater osmotic pressure. This result correlates well with the data described by the authors of [41], who studied the dehydration of porcine skin with PEG-200 and PEG-400 and showed that the dehydrating effect of PEG-200 in the first 30 min of dehydration was stronger than that of PEG-400. Furthermore, in the initial period, dehydration in the presence of PEG-300 proceeded more rapidly than in the presence of PEG-400. The values and rates of the longitudinal and transverse compression of the skin samples also significantly differed due to the structure of the skin, in which the collagen and elastin fibers constituting its frame are arranged in parallel to the skin surface. It can be seen that the longitudinal compression of skin samples practically ended approximately after 1 h of exposure to PEG-300 and PEG-400, whereas the transverse compression continued for the entire 2 h of measurements, which was especially noticeable in the case of PEG-400. Apparently, the decrease in the length of the fibers is less pronounced compared to the decrease in the interstitial space between them due to osmotic dehydration of the tissue.

Although PEG-400 caused a more pronounced decrease in the volume of the skin samples in general, due to the differences in the compression rates for PEG-300 and PEG-400 the former caused a greater reduction in the volume of skin samples than PEG-400 in the first 30 min of dehydration.

Thus, it can be concluded that, in the presence of PEG-300, skin is dehydrated more rapidly than in the presence of PEG-400 due to the lower viscosity and

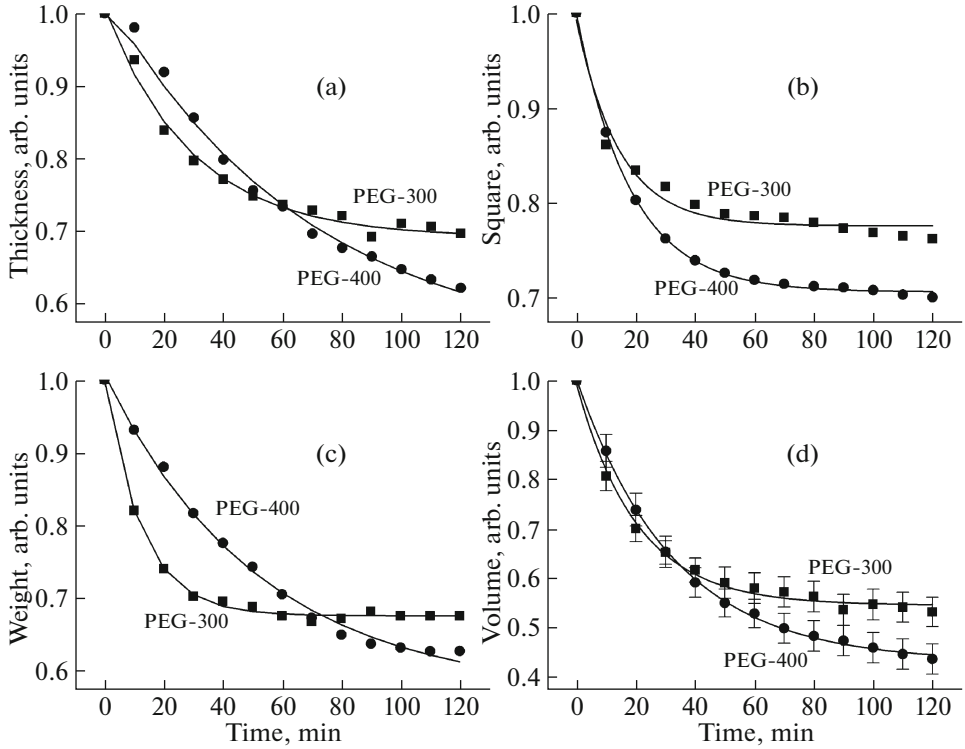

Fig. 3. Kinetics of alterations of (a) thickness, (b) square, (c) weight, and (d) volume of skin samples. The points correspond to the experimental data, and the solid line shows the approximation according to Eq. (14). The approximation parameters are shown in Table 3.

Table 3. Parameters of skin dehydration under the action of PEG-300 and PEG-400

Dehydration index		Clearing agent	
		PEG-300	PEG-400
Weight/dehydration	B^W	0.32 ± 0.01	0.43 ± 0.01
	τ^W, min	12.5 ± 0.4	52.1 ± 4.1
	B_0^W	0.68 ± 0.01	0.57 ± 0.01
Thickness/transversal compression	B^l	0.31 ± 0.01	0.47 ± 0.03
	τ^l, min	29.4 ± 3.5	68.5 ± 9.6
	B_0^l	0.69 ± 0.01	0.53 ± 0.03
Area/longitudinal compression	B^S	0.22 ± 0.01	0.29 ± 0.01
	τ^S, min	14.5 ± 1.8	18.2 ± 0.4
	B_0^S	0.78 ± 0.01	0.71 ± 0.01
Volume/dehydration	B^V	0.45 ± 0.01	0.57 ± 0.01
	τ^V, min	20.3 ± 1.2	32.5 ± 0.8
	B_0^V	0.55 ± 0.01	0.43 ± 0.01

the larger osmotic pressure of PEG-300, whereas the degree of dehydration by PEG-400 is greater compared to PEG-300. The lower degree of skin dehydration in the presence of PEG-300 is apparently due to the decrease in its hygroscopicity with increasing molecular weight of PEG (i.e., when penetrating deeply into the skin, PEG-300 due to its higher hygroscopicity [18, 19] more effectively binds the interstitial water and stops the process of osmotic dehydration).

Figures 4 and 5 show the representative spectra and the kinetics of alteration the collimated transmittance of skin samples under the action of PEG-300 and PEG-400 in the range of 500–900 nm for 2 h. As can be seen from Fig. 4, at the initial time moment, skin is a medium that is almost nontransparent in the visible and near infrared regions of the spectrum. Upon the penetration of OCA into the interstitial fluid and simultaneous dehydration of the skin, a decrease in the scattering and, respectively, an increase in the collimated transmittance of samples are observed. It can be seen that the optical clearing of the skin samples occurs in the entire range of wavelengths. Figure 5 clearly shows that the collimated transmittance increases primarily in the first 60–70 min of measurements. Then, the process is stabilized, and after approximately 80–90 min of skin clearing no substantial increase in the collimated transmittance is observed.

The degree of optical clearing is one of the most important parameters characterizing the comparative

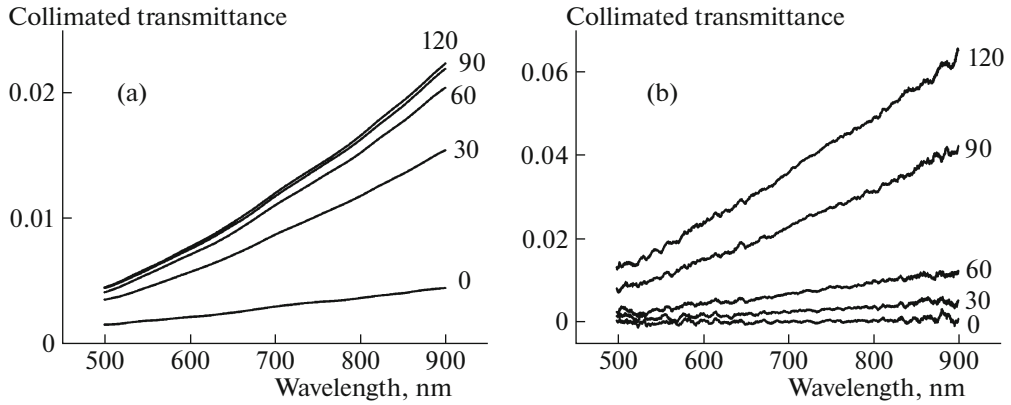

Fig. 4. Representative spectra of collimated transmittance in rat skin ex vivo measured at different time intervals after placing in (a) PEG-300 and (b) PEG-400.

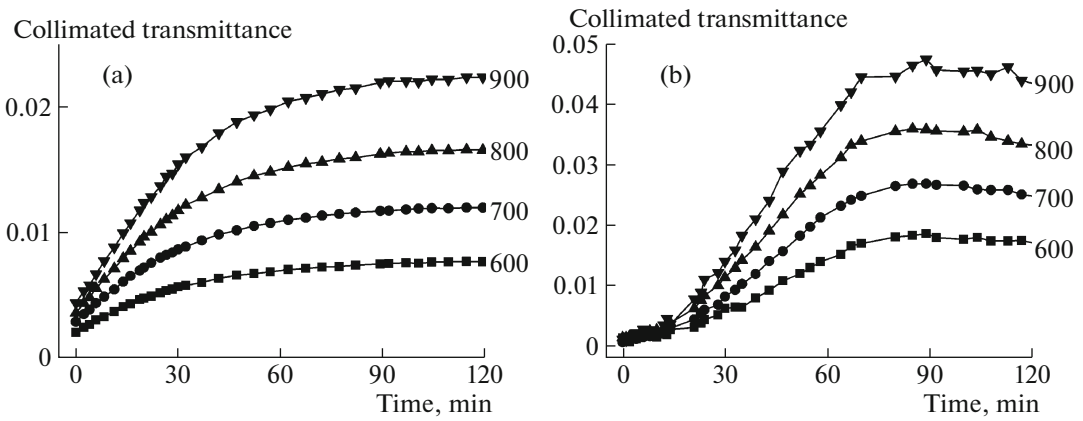

Fig. 5. Representative kinetics of alteration of the collimated transmittance coefficient of rat skin ex vivo under the action of (a) PEG-300 and (b) PEG-400 measured at different wavelengths.

efficacy and practical value of various clearing agents. The rate (efficiency) of optical clearing of the skin was estimated in three spectral ranges using the expression $OC_{ef} = \frac{\mu_{s0} - \mu_s(t)}{\mu_{s0}}$, where μ_{s0} is the scattering coefficient at the initial time and $\mu_s(t)$ is the scattering coefficient value at time t of the optical clearing of the skin. The results are summarized in Table 4.

As can be clearly seen from Table 4, the efficiency of optical clearing increases with an increase in the wavelength, e.g., from 0.16 ± 0.12 (range 600–700 nm) to 0.21 ± 0.15 (range 800–900 nm) 10 min after the start of exposure to PEG-300 or from 0.31 ± 0.14 (range 600–700 nm) to 0.36 ± 0.11 (range 800–900 nm) 60 min after the start of exposure to PEG-400. This behavior can be explained by the fact that, as the wavelength increases, the difference between the values of the refractive index of skin scatterers (9) and the values of the refractive index of the interstitial fluid (8) decreases.

The comparison of the efficiency of optical clearing caused by PEG-300 and PEG-400 shows that, during the first 30 min, OC_{ef} for PEG-300 was greater than that for PEG-400. This difference can be explained by the fact that, in the initial period of time, function $\frac{\varphi_S(t)(1-\varphi_S(t))^3}{1+\varphi_S(t)}$ (the so-called scatterer packing factor (see (10)) in the presence of PEG 300 takes lower values than in the presence of PEG-400. Since in the initial period of time the concentration of PEG in the skin is relatively low (i.e., the scattering cross section changes only slightly), the optical clearing is determined mainly by the dehydration mechanism. The results correlate well with the data of [14], the authors of which showed that the clearing effect increased with increasing molecular weight of PEG.

The diffusion coefficient of PEG in the skin was estimated on the basis of the analysis of the kinetics of alteration of the collimated transmittance of rat skin ex vivo using the algorithm presented in the section Estimation of Diffusion Coefficients of OCA in Skin tak-

Table 4. Optical clearing of skin under the action of PEG-300 and PEG-400

Measurement time, min	Spectral range					
	600–700 nm		700–800 nm		800–900 nm	
	PEG-300	PEG-400	PEG-300	PEG-400	PEG-300	PEG-400
5	0.11 ± 0.09	0.07 ± 0.07	0.11 ± 0.10	0.06 ± 0.06	0.14 ± 0.12	0.07 ± 0.04
10	0.16 ± 0.12	0.10 ± 0.08	0.18 ± 0.13	0.12 ± 0.11	0.21 ± 0.15	0.12 ± 0.09
15	0.19 ± 0.13	0.16 ± 0.12	0.24 ± 0.15	0.19 ± 0.16	0.27 ± 0.17	0.17 ± 0.13
30	0.24 ± 0.15	0.24 ± 0.16	0.28 ± 0.15	0.28 ± 0.18	0.32 ± 0.18	0.28 ± 0.16
60	0.27 ± 0.15	0.31 ± 0.14	0.32 ± 0.16	0.35 ± 0.12	0.35 ± 0.17	0.36 ± 0.11
120	0.28 ± 0.13	0.37 ± 0.15	0.32 ± 0.13	0.40 ± 0.11	0.36 ± 0.14	0.42 ± 0.10

ing into account the alteration in the kinetics of structural and geometrical parameters of the skin. The measured values of the diffusion coefficient reached $(1.83 \pm 2.22) \times 10^{-6}$ cm^2/s for PEG-300 and $(1.70 \pm 1.47) \times 10^{-6}$ cm^2/s for PEG-400. The resulting value of the diffusion coefficient of PEG-300 in the skin was greater than that of PEG-400, and PEG-300/PEG-400 diffusion coeffitients ratio is well matched to data of their diffusion in water [27]: 5.08×10^{-6} cm^2/s (for PEG-300) and 4.45×10^{-6} cm^2/s (for PEG-400) and the diffusion coefficients of PEG-300 and PEG-400 in the corneal layer of the skin epidermis [20]: $(4.5 \pm 2.9) \times 10^{-9}$ cm^2/h (for PEG-300) and $(3.7 \pm 2.5) \times 10^{-9}$ cm^2/h (for PEG-400), which after recalculation gives ~1.25×10^{-12} cm^2/s (for PEG-300) and ~1.03×10^{-12} cm^2/s (for PEG-400).

CONCLUSIONS

These results demonstrate the efficacy of PEG as a clearing agent to control the scattering characteristics of the skin. In particular, an increase in the collimated light transmittance through the skin in the spectral range of 500–900 nm, a decrease in the diffusion rate of PEG, an increase in the efficiency of optical clearing of the skin, and the enhancement of the transversal compression of the skin were observed with increasing molecular weight of PEG. The measured values of the diffusion coefficients of PEG-300 and PEG-400 in rat skin ex vivo were $(1.83 \pm 2.22) \times 10^{-6}$ and $(1.70 \pm 1.47) \times 10^{-6}$ cm^2/s, respectively.

ACKNOWLEDGMENTS

This study was supported by the Russian Science Foundation, project no. 14-15-00186.

REFERENCES

1. D. A. Zimnyakov and V. V. Tuchin, Quantum Electron. **32**, 849 (2002).
2. V. V. Tuchin, *Lasers and Fiber Optics in Biomedical Science* (Fizmatlit, Moscow, 2010) [in Russian].
3. V. V. Tuchin, *Tissue Optics: Light Scattering Methods and Instruments for Medical Diagnosis,* SPIE Press Monograph, Vol. 166 (Fizmatlit, Moscow, 2012; SPIE Publ., 2007).
4. V. V. Tuchin, Laser Phys. **15**, 1109 (2005).
5. E. A. Genina, A. N. Bashkatov, and V. V. Tuchin, Expert Rev. Med. Dev. **7**, 825 (2010).
6. D. Zhu, K. Larin, Q. Luo, and V. V. Tuchin, Laser Photon. Rev. **7**, 732 (2013).
7. E. A. Genina, A. N. Bashkatov, Yu. P. Sinichkin, I. Yu. Yanina, and V. V. Tuchin, J. Biomed. Photon. Eng. **1**, 22 (2015).
8. C. G. Rylander, O. F. Stumpp, T. E. Milner, N. J. Kemp, J. M. Mendenhall, K. R. Diller, and A. J. Welch, J. Biomed. Opt. **11**, 041117 (2006).
9. A. T. Yeh and J. Hirshburg, J. Biomed. Opt. **11**, 014003 (2006).
10. X. Wen, Z. Mao, Z. Han, V. V. Tuchin, and D. Zhu, J. Biophoton. **3**, 44 (2010).
11. E. A. Genina, A. N. Bashkatov, Yu. P. Sinichkin, and V. V. Tuchin, Opt. Spectrosc. **109**, 225 (2010).
12. J. Wang, N. Ma, R. Shi, Y. Zhang, T. Yu, and D. Zhu, IEEE J. Sel. Top. Quantum Electron. **20**, 7101007 (2014).
13. Y. Liu, X. Yang, D. Zhu, and Q. Luo, Opt. Lett. **38**, 4236 (2013).
14. Z. Mao, D. Zhu, Y. Hu, X. Wen, and Z. Han, J. Biomed. Opt. **13**, 021104 (2008).
15. Y. Ding, J. Wang, Z. Fan, D. Wei, R. Shi, Q. Luo, D. Zhu, and X. Wei, Biomed. Opt. Express **4**, 2518 (2013).
16. H. Zhong, Z. Guo, H. Wei, L. Guo, C. Wang, Y. He, H. Xiong, and S. Liu, Photochem. Photobiol. **86**, 732 (2010).
17. E. A. Genina, A. N. Bashkatov, E. A. Kolesnikova, M. V. Basko, G. S. Terentyuk, and V. V. Tuchin, J. Biomed. Opt. **19**, 021109 (2014).
18. J. K. Gao, *Polyethylene Glycol as an Embedment for Microscopy and Histochemistry* (CRC, Boca Raton, FL, 1993).
19. *Handbook of Pharmaceutical Excipients,* Ed. by R. C. Rowe, P. J. Sheskey, and M. E. Quinn (Pharmaceut. Press, Amer. Pharmacists Assoc., 2009).
20. I. Jakasa, M. M. Verberk, M. Esposito, J. D. Bos, and S. Kezic, J. Invest. Dermatol. **127**, 129 (2007).
21. K. M. Hamalainen, K. Kontturi, S. Auriola, L. Murtomaki, and A. Urtti, J. Control. Release **49**, 97 (1997).
22. L. Weng, S. Liang, L. Zhang, X. Zhang, and J. Xu, Macromolecules **38**, 5236 (2005).
23. H. Gursahani, J. Riggs-Sauthier, J. Pfeiffer, D. Lechuga-Ballesteros, and C. S. Fishburn, J. Pharmaceut. Sci. **98**, 2847 (2009).
24. http://www.sigmaaldrich.com/catalog/product/fluka/81160?lang=en&region=RU
25. http://www.sigmaaldrich.com/catalog/product/fluka/81170?lang=en&region=RU
26. N. P. Money, Plant Physiol. **91**, 766 (1989).
27. L. Johansson, U. Skantze, and J.-E. Lofroth, Macromolecules **24**, 6019 (1991).
28. P. Schiebener, J. Straub, J. M. H. L. Sengers, and J. S. Gallagher, J. Phys. Chem. Ref. Data **19**, 677 (1990).
29. V. V. Tuchin, *Optical Clearing of Tissues and Blood,* SPIE Press Monographs, Vol. 154 (SPIE, Bellingham, 2005).
30. A. N. Bashkatov, E. A. Genina, and V. V. Tuchin, in *Handbook of Optical Sensing of Glucose in Biological Fluids and Tissues,* Ed. by V. V. Tuchin (CRC, Taylor and Francis, London, 2009), p. 587.
31. D. W. Leonard and K. M. Meek, Biophys. J. **72**, 1382 (1997).

32. A. N. Bashkatov, E. A. Genina, and V. V. Tuchin, J. Innovative Opt. Health Sci. **4**, 9 (2011).
33. A. N. Bashkatov, E. A. Genina, Yu. P. Sinichkin, V. I. Kochubey, N. A. Lakodina, and V. V. Tuchin, Biophysical J. **85**, 3310 (2003).
34. J. M. Schmitt and G. Kumar, Appl. Opt. **37**, 2788 (1998).
35. C. F. Bohren and D. R. Huffman, *Absorption and Scattering of Light by Small Particles* (Wiley, New York, 1983).
36. Y. Huang and K. M. Meek, Biophys. J. **77**, 1655 (1999).
37. H. Fischer, I. Polikarpov, and A. F. Craievich, Protein Sci. **13**, 2825 (2004).
38. A. N. Bashkatov, E. A. Genina, I. V. Korovina, V. I. Kochubey, Yu. P. Sinichkin, and V. V. Tuchin, Proc. SPIE—Int. Soc. Opt. Eng. **4224**, 300 (2000).
39. H. A. Linares, C. W. Kischer, M. Dobrkovsky, and D. L. Larson, J. Invest. Dermatol. **59**, 323 (1972).
40. W. H. Press, S. A. Tuekolsky, W. T. Vettering, and B. P. Flannery, *Numerical Recipes in C: The Art of Scientific Computing* (Cambridge Univ. Press, Cambridge, New York, 1992).
41. T. Yu, X. Wen, V. V. Tuchin, Q. Luo, and D. Zhu, J. Biomed. Opt. **16**, 095002 (2011).

Translated by M. Batrukova